interferometer which then provides us with an estimate of the scan width that is accurate to about 10%. A molecular beam spectrum of the same rovibrational line depicted in the Figure 1 photoacoustic scan is displayed in Figure 2. The observed linewidth is 3 ± 0.2 Mhz. It is limited by contributions of approximately 1 Mhz each from the laser bandwidth, the residual Doppler broadening from the molecular beam divergence, and the transit time broadening due to the rapid passage of the molecular beam through the 1-mm-diameter laser beam. The slight assymmetry of the molecular beam line shape is probably due to imperfect alignment of the Fabry Perot buildup cavity. We have also observed the $2_{-2} \leftarrow 1_{-1}$ rovibronic transition in H_2O on the molecular beam. Its line shape is similar to that displayed in Figure 2.

It must be emphasized that the H_2O spectra of Baumann and Mecke exhibit sharp, clearly resolved rovibrational structure without a hint of the massive line broadening that characterizes overtone spectra of many molecules. Their Doppler limited resolution was on the order of 1 Ghz. From the present experiment we are able to conclude that the H_2O (301) ← (000) overtone transitions are at least as sharp as a few Mhz, implying that the excited-state lifetime could be no shorter than about 300 ns.

Now that it has been demonstrated that a $\Delta v = 4$ overtone transition in the near-infrared can be detected under molecular beam conditions, polyatomic molecules that are somewhat larger than H_2O will be investigated with this apparatus. The densities of vibrational states at the levels excited in these molecules will be larger than for the case of H_2O, and it remains to be seen whether line broadening or simply spectral congestion will be evident in their molecular beam overtone spectra. The present results indicate an experimental procedure capable of distinguishing these two possibilities.

Acknowledgment. J. P. Reilly thanks Leo Hollberg for helpful discussions about buildup cavities. Also the authors thank D. Brabson for his contributions toward this effort. This work has been supported by the National Science Foundation under Grant CHE-81-16962.

FEATURE ARTICLE

Making and Breaking Bonds in the Solid State: The $ThCr_2Si_2$ Structure

Roald Hoffmann* and Chong Zheng

Department of Chemistry and Materials Science Center, Cornell University, Ithaca, New York 14853
(Received: April 8, 1985)

Among the many examples of the $ThCr_2Si_2$ structural type is a set of AB_2X_2 structures, B = transition metal, X = group 14 or 15 element, in which one X···X contact varies over the range of bonding between no bond and a fully formed X–X single bond. The tuning is provided by variation in the transition metal, X–X bonding being promoted by metals on the right-hand side of the periodic table. We begin with chemical construction of the bonding in B_2X_2 layers. When these two-dimensional layers are stacked, narrow X–X σ and σ^* bands result. The σ^* level is filled (no X–X bond) or empty (X–X bonding) depending on the Fermi level of the transition-metal B layer.

More than 400 compounds of AB_2X_2 stoichiometry adopt the $ThCr_2Si_2$ type structure.[1] In these A is typically a rare earth, alkaline earth, or alkali element; B is a transition-metal or main-group element, and X comes from group 15, 14, and occasionally 13.[3,4] Since the synthesis of AB_2X_2 with A = a rare-earth element by Parthé, Rossi, and their co-workers[2] the unusual physical properties exhibited by these solids have attracted much attention. Physicists speak with enthusiasm of valence fluctuation,[3] p-wave or heavy fermion superconductivity[4] and of many peculiar magnetic properties[5] of these materials. But the underlying nature of the chemical bonding in these remarkable compounds has not been explored in detail. In this first of a series of papers on the versatile AB_2X_2 system, we are going to analyze the making and breaking of a single bond, the X–X bond, in these compounds. In the process we will illustrate how the computational methods of solid-state physics, the analytical tools of quantum chemistry, and chemical intuition can come together to yield an understanding of a seemingly complex material.

X–X Pair Formation in $ThCr_2Si_2$ Type AB_2X_2 Structures

The $ThCr_2Si_2$ structure type of AB_2X_2 stoichiometry compounds is shown in **1**. It consists of $B_2X_2^{2-}$ layers interspersed with A^{2+} layers. The bonding between A and B_2X_2 layers appears largely ionic, which is why we write the charge partitioning as A^{2+} and $B_2X_2^{2-}$. But in the $B_2X_2^{2-}$ layer there is indication not only of covalent B–X bonding, but also some metal–metal B–B bonding.

There are several alternative ways to describe the layer structure. For instance the B_2X_2 layer may be thought of as being built up by sharing four of the six edges of a BX_4 tetrahedron by

(1) (a) Ban, Z.; Sikirica, M. *Acta Crystallogr.* **1965**, *18*, 594. For two papers with leading references, see ref 1b, c. (b) Marchand, R.; Jeitschko, W.; *J. Solid State Chem.* **1978**, *24*, 351. Jeitschko, W.; Jaberg, B. *Ibid.* **1980**, *35*, 312. Hofmann, W. K.; Jeitschko, W. *Ibid.* **1984**, *51*, 152. (c) Pearson, W. B. *Ibid.* **1985**, *56*, 278.

(2) (a) Rieger, W.; Parthé, E. *Monatsh. Chem.* **1969**, *100*, 444. (b) Rossi, D.; Marazza, R.; Ferro, R. *J. Less-Common Met.* **1978**. *58*, 203.

(3) (a) "Valence Instabilities"; Wachter, P., Boppart, H., Eds.; North-Holland: Amsterdam, 1982. (b) Lawrence, J. M.; Riseborough, P. S.; Parks, R. D. *Rep. Prog. Phys.* **1981**, *44*, 1.

(4) (a) Steglich, F.; Aarts, J.; Bredl, C. D.; Lieke, W.; Meschede, D.; Franz, W.; Schäfer, H. *Phys. Rev. Lett.* **1979**, *43*, 1892. (b) Lieke, W.; Rauchschwalbe, V.; Bredl, C. D.; Steglich, F.; Aarts, J.; de Boer, F. R. *J. Appl. Phys.* **1982**, *53*, 2111. (c) Assmus, W.; Herrmann, M.; Rauchschwalbe, U.; Regel, S.; Lieke, W.; Spille, H.; Horn, S.; Weber, G.; Steglich, F.; Cordier, G. *Phys. Rev. Lett.* **1984**, *52*, 469 and references cited therein.

(5) See, for example: Batlogg, B.; Remeika, J. P.; Cooper, A. S.; Fisk, Z. *Bull. Am. Phys. Soc.* **1984**, *29*, 404.

0022-3654/85/2089-4175$01.50/0

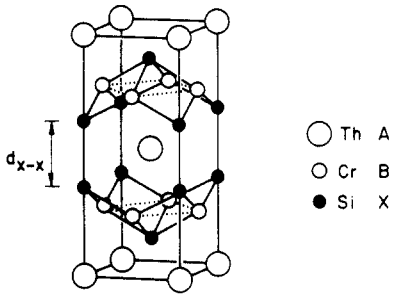

1

infinite extension in two dimensions, as in **2**. Alternatively we

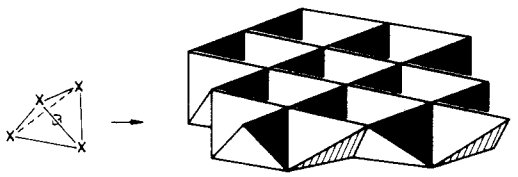

2

may describe the coordination at each metal B atom as approximately tetrahedral in X, with four additional near-neighbor B···B contacts. The main-group X atoms are at the apex of a square pyramid of B atoms. Still another way to describe this lovely layer is to imagine a perfect square-planar two-dimensional lattice of metal atoms, above and below the fourfold hollows of which lie the main-group X atoms. This is shown in **3** below.

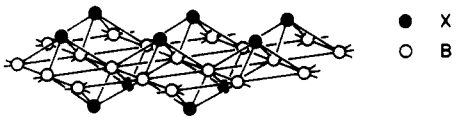

3

There is a long X···X contact within a layer, but what becomes the main focus of this paper is a remarkable tunable X···X contact *between* two layers, along one of the edges of the tetragonal unit cell depicted in **1**. This contact, d_{X-X}, is the primary variable geometrical factor in these molecules. In Table I we list some of the known $ThCr_2Si$ structures. This is not a complete list, only a selection. A trend is apparent: for the same cation A and the same main-group element X, d_{X-X} decreases as the transition metal B moves from the left-hand side to the right-hand side in the Periodic Table. One series of these compounds, studied by Mewis,[6] is singled out in Table II.

For reference the P–P distance in P_4 is 2.21[21] and 2.192 Å in Me_2P–PMe_2.[22] The P–P single bond distance is remarkably constant at 2.19–2.26 Å.[22,23] The P≡P triple bond and P=P double bond lengths are around 1.87[24] and 2.03 Å.[25,26] It is clear

TABLE I: Crystal Parameters of Some of the $ThCr_2Si_2$ Structure Compounds

AB_2X_2	a, Å	d_{B-X}, Å	XBX angle	d_{X-X}, Å	ref
$CaCu_{1.75}P_2$	4.014	2.381	114.90	2.251	6
$CaNi_2P_2$	3.916	2.293	117.28	2.297	6
$CaCo_2P_2$	3.858	2.257	117.44	2.454	6
$CaFe_2P_2$	3.855	2.24	118.74	2.710	6
$SrCu_{1.75}P_2$	4.166	2.431	117.93	2.297	6
$SrCo_2P_2$	3.794	2.240	115.75	3.424	6
$SrFe_2P_2$	3.825	2.251	116.34	3.434	6
$BaFe_2P_2$	3.840	2.259	116.41	3.842	6
$BaMn_2P_2$	4.037	2.455	110.61	3.737	6
$BaRh_2B_2$	3.915	2.106	136.71	*a*	7
$CaNi_2As_2$	4.065	2.356	119.24	2.59	8
$SrNi_2As_2$	4.154	2.377	121.80	2.83	8
KFe_2As_2	3.842	2.389	107.05	*a*	9
KRh_2As_2	3.987	2.424	110.66	*a*	9
$BaZn_2P_2$	4.019	2.486	107.86	*a*	10
$EuCo_2P_2$	3.765	2.233	114.92	3.27	1b
$LaCo_2B_2$	3.616	2.21	109.79	2.55	11
YCo_2B_2	3.561	2.13	113.42	2.34	11
$LiCu_2P_2$	3.887	2.35	111.59	2.14	12
$BaMn_2As_2$	4.15	2.56	108.30	3.75	13
$CaMn_2Ge_2$	4.17	2.50	113.02	2.60	14
$SrMn_2Ge_2$	4.30	2.55	114.96	2.63	14
$BaMn_2Ge_2$	4.47	2.63	116.38	2.74	14
$BaMn_2Sn_2$	4.74	2.73	120.48	2.94	14
$CaCo_2Ge_2$	4.00	2.35	116.65	2.65	14
$SrCo_2Ge_2$	4.08	2.38	117.99	2.88	14
$CaNi_2Ge_2$	4.084	2.36	119.82	2.61	14
$SrNi_2Ge_2$	4.17	2.38	122.34	2.83	14
$SrCu_2Ge_2$	4.27	2.47	119.62	2.70	14
$SrZn_2Ge_2$	4.37	2.60	114.36	2.50	14
$CaAu_2Si_2$	4.32	2.43	125.47	2.77	14
$SrAu_2Si_2$	4.37	2.47	124.41	2.78	14
$SrAg_2Sn_2$	4.67	2.80	113.01	2.79	14
$BaAu_2(Au, Ge)_2$	4.65	2.67	121.10	2.64	15
$SrAl_2Pb_2$	4.46	2.65	114.60	2.73	15
$EuFe_2Si_2$	3.970	2.353	115.04	2.53	16
$EuCo_2Si_2$	3.921	2.315	115.74	2.46	16
$EuNi_2Si_2$	4.008	2.338	117.99	2.409	16
$EuCu_2Si_2$	4.057	2.376	117.24	2.477	16
$EuNiSi_3$	4.150	2.399	119.75	2.409	16
$EuNi_2Ge_2$	4.144	2.424	117.47	2.724	16
$EuCu_2Ge_2$	4.215	2.46	117.89	2.749	16
$CeNi_2Si_2$	4.027	2.23	129.08	2.87	17
$LnPt_2Si_2$	4.28–4.08	~2.4	~120.00	~2.55	18
$LaAg_2Si_2$	4.295	2.526	116.45	2.617	19
$LaAu_2Si_2$	4.337	2.514	119.21	2.24	19
$SmAg_2Si_2$	4.169	2.476	114.67	2.63	19
$SmAu_2Si_2$	4.260	2.48	118.38	2.237	19
$BaMg_2Si_2$	4.65	2.78	113.51	2.48	20
$BaMg_2Ge_2$	4.67	2.80	113.01	2.58	20
$CaCu_2Si_2$	4.04	2.42	113.17	2.32	20
$SrCu_2Si_2$	4.20	2.47	116.47	2.42	20
$CaCu_2Ge_2$	4.139	2.45	115.27	2.48	20

[a] No X–X bonding.

TABLE II: X–X Distance in Some Phosphide Compounds of the AB_2X_2 Type

AB_2X_2	d_{X-X}, Å	AB_2X_2	d_{X-X}, Å
$CaCu_{1.75}P_2$	2.25	$SrCu_{1.75}P_2$	2.30
$CaNi_2P_2$	2.30	$SrCo_2P_2$	3.42
$CaCo_2P_2$	2.45	$SrFe_2P_2$	3.43
$CaFe_2P_2$	2.71		

(6) Mewis, A. *Z. Naturforsch., B* **1980**, *35B*, 141.
(7) Jung, W. *Z. Naturforsch., B* **1979**, *34B*, 1221.
(8) Mewis, A.; Distler, A. *Z. Naturforsch., B* **1980**, *35B*, 391.
(9) Rôzsa, S.; Schuster, H.-U. *Z. Naturforsch., B* **1981**, *36B*, 1668.
(10) Klüfers, P.; Mewis, A. *Z. Naturforsch., B* **1978**, *33B*, 151.
(11) Nihara, K.; Shishido, T.; Yajima, S. *Bull. Chem. Soc. Jpn.* **1973**, *46*, 1137.
(12) Schlenger, H.; Jacobs; H.; Juza, R. *Z. Anorg. Allg. Chem.*, **1971**, *385*, 177.
(13) Brechtel, E.; Cordier, G.; Schäfer, H. *Z. Naturforsch., B* **1978**, *33B*, 820.
(14) Dörrscheidt, W.; Niess, N.; Schäfer, H. *Z. Naturforsch., B* **1976**, *31B*, 890.
(15) May, N.; Schäfer, H. *Z. Naturforsch., B* **1972**, *27B*, 864.
(16) Mayer, I.; Felner, I. *J. Phys. Chem. Solids* **1977**, *38*, 1031.
(17) Bodak, O. I.; Gladyshevskii, E. I.; Kripyakevich, P. I. *Izv. Akad. Nauk SSSR Neorg. Mater.* **1966**, *2*, 2151.
(18) Mayer, I.; Yetor, P. D. *J. Less-Common Met.* **1977**, *55*, 171.
(19) Mayer, I.; Cohen, J.; Felner, I. *J. Less-Common Met.* **1973**, *30*, 181.
(20) Eisenmann, B.; May, N.; Müller, W.; Schäfer, H.; Weiss, A.; Winter, G.; Ziegleder, G. *Z. Naturforsch. B* **1970**, *25B*, 1350.
(21) Maxwell, L. R.; Hendricks, S. B.; and Mosley, V. M. *J. Chem. Phys.* **1935**, *3*, 699.
(22) McAdam, A.; Beagley, B.; Hewitt, T. G. *Trans. Faraday Soc.* **1970**, *66*, 2732.
(23) (a) Emsley, J.; Hall, D. "The Chemistry of Phosphorus"; Harper and Row: London, 1976. (b) An interesting molecule, $P_{12}(i\text{-}Pr)_4$, has a range of P–P single bond lengths between 2.182 and 2.261 Å. See: Baudler, M. *Z. Chem.* **1984**, *24*, 352.

that the short distances in these phosphides are characteristic of a full P–P single bond. The long contacts, such as 3.43 Å, imply essentially no bonding at all. All the compounds in Table I with a nonbonding X···X separation contain metals from the left-hand side of the Periodic Table (except $BaZn_2P_2$, to which we will return). Clearly there is an electronic effect at work here—a X···X bond is made or broken in the solid state. We would like to understand how and why this happens.

Bonding within a B_2X_2 Layer

We approach the AB_2X_2 structure, represented by a typical $BaMn_2P_2$ compound, in stages. First we will look at a single two-dimensional $Mn_2P_2^{2-}$ layer. Then we will form a three-dimensional $Mn_2P_2^{2-}$ sublattice by bringing many such layers together in the third dimension. Finally, we may insert the Ba^{2+} counterions into the structure.

Consider a single Mn_2P_2 layer (**2** ≡ **3**). The Mn–P distance is 2.455 Å, and the Mn–Mn distance in the square metal lattice is 2.855 Å. The latter is definitely in the metal–metal bonding range, and so a wide-band, delocalized picture is inevitable. But in some hierarchy or ranking of interactions it is clear that Mn–P bonding is stronger than Mn–Mn. So let us construct this solid conceptually, or think of it, in terms of first turning an Mn–P bonding, and then Mn–Mn interaction.

The local coordination environment at each Mn is approximately tetrahedral. If we had a discrete tetrahedral Mn complex, e.g. $Mn(PR_3)_4$, we might expect a qualitative bonding picture such as **4**. Four phosphine lone pairs, $a_1 + t_2$ in symmetry, interact

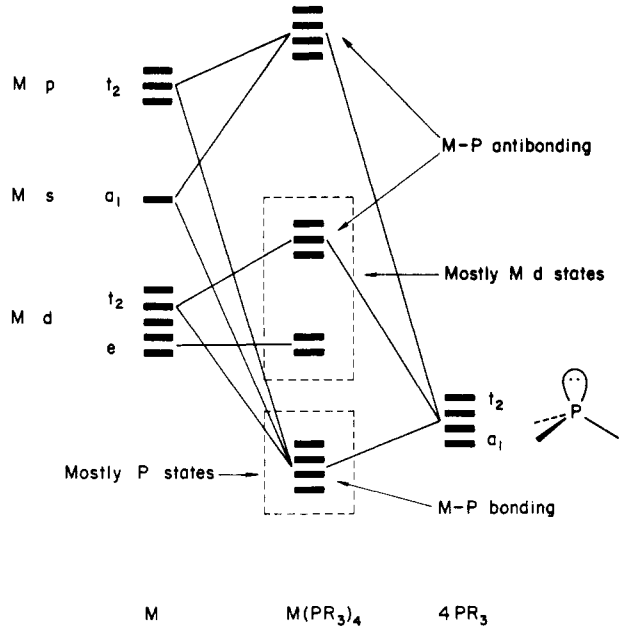

4

with their symmetry match, mainly Mn 4s and 4p, but also with the t_2 component of Mn 3d set. Four orbitals, mainly on P, P–Mn σ bonding, go down. Four orbitals, mainly on Mn, P–Mn σ antibonding, go up. The Mn d block splits in the expected two below three way.

Something like this *must* happen in the solid. In addition there are Mn–Mn bonding contacts in the layer, and these will lead to dispersion in those bands which are built up from orbitals con-

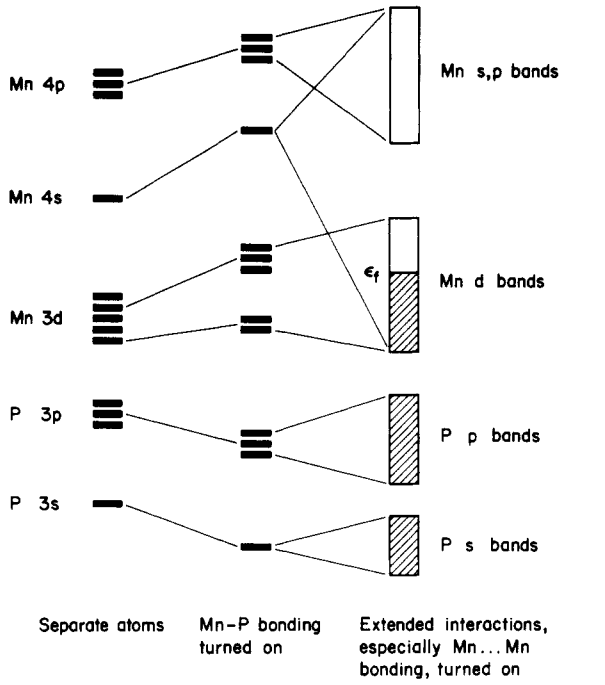

Figure 1. Schematic picture of the $Mn_2P_2^{2-}$ layer band structure as derived by first turning on local Mn–P interactions and then the two-dimensional periodicity and Mn–Mn interactions.

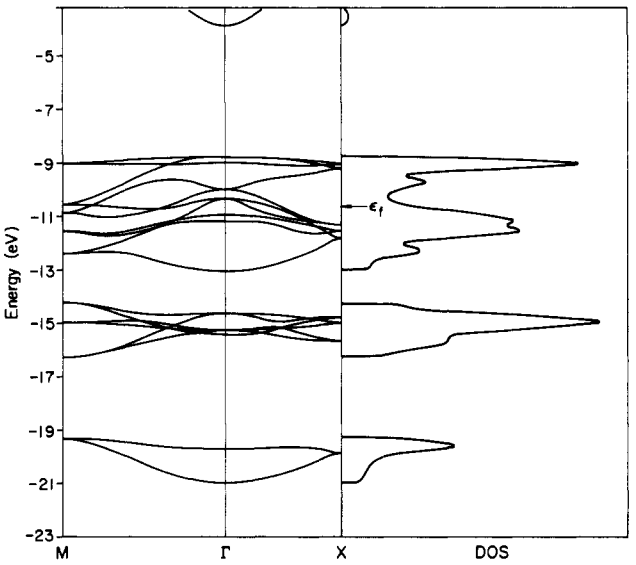

Figure 2. Band structures and total DOS of a single $Mn_2P_2^{2-}$ layer.

taining substantial metal character. The combined construction is shown in Figure 1.

Can we see this local, very chemical bonding construction in a delocalized band structure? Most certainly, as we will now show. We are going to use throughout this paper tight-binding calculations of the extended Hückel type, with parameters described in the Appendix. The calculated band structure and total density of states of a single $Mn_2P_2^{2-}$ layer are illustrated in Figure 2. The bands correspond to the final translationally delocalized picture, the right-hand side of Figure 1. They are not very informative chemically until we apply some decomposition and partitioning analyses to them.

Let us begin by constructing the Mn_2P_2 layer from separate Mn and P films, in an attempt to model the primary bonding effect, Mn–P interaction. This is done in Figure 3. At left is the P sublattice. We see P 3s (around −19 eV) and P 3p (around −14 eV) bands. Both are narrow because the P atoms are ~4 Å apart. The Mn sublattice (middle of Figure 3) shows a nicely dispersed density of states (DOS). The Mn–Mn separation is only 2.855 Å. Thus we have a two-dimensional metal, with a familiar

(24) (a) Corbridge, D. E. C. "Phosphorus"; Elsevier: Amsterdam, 1978. (b) Bowen, H. J. M. et al. "Tables of Interatomic Distances and Configuration in Molecules and Ions"; The Chemical Society: London, 1958; Special Publication No. 11.

(25) (a) Yoshifuji, M.; Shima, I.; Inamoto, N.; Hirotsu, K.; Higuchi, T. *J. Am. Chem. Soc.* **1981**, *103*, 4587. (b) Flynn, K. M.; Olmstead, M. M.; Power, P. P. *Ibid.* **1983**, *105*, 2085.

(26) Niecke, E.; Ruger, R.; Lysek, M.; Pohl, S.; Schoeller, W.; *Angew. Chem.* **1983**, *95*, 495; *Angew. Chem., Int. Ed. Engl.* **1983**, *22*, 486. Niecke, E.; Rüger, R. *Angew. Chem.* **1983**, *95*, 154; *Angew. Chem., Int. Ed. Engl.* **1983**, *22*, 155.

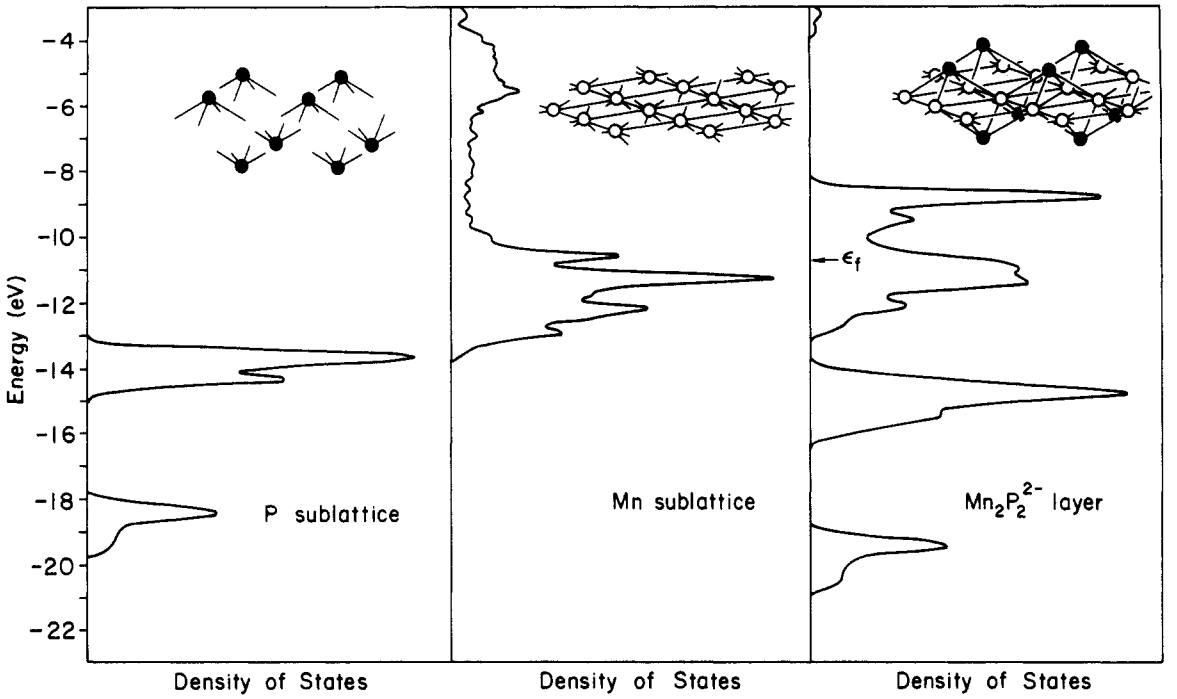

Figure 3. Total DOS of the P sublattice (left), the Mn sublattice (middle), and the composite $Mn_2P_2^{2-}$ layer lattice (right).

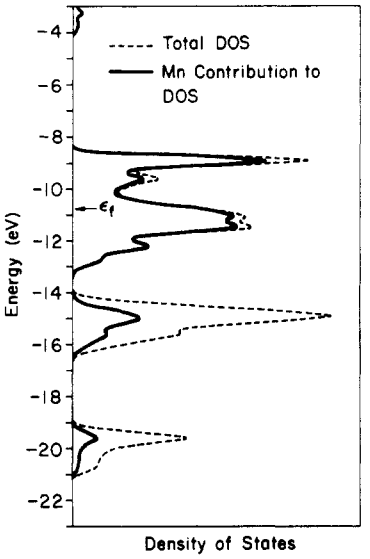

Figure 4. Total DOS of the composite $Mn_2P_2^{2-}$ layer lattice (dashed line) and the contribution of Mn orbitals to that DOS (solid line).

wide s, p plus narrow d band pattern. The bottom part of the DOS in the middle of Figure 3 is the 3d band; the top is the lower part of the 4s, 4p band. At right in Figure 3 is the density of states of the composite Mn_2P_2 layer. Note how the individual P and Mn bunches of states repel each other on forming the composite lattice. There is no more graphic way of showing that what happens in the inorganic solid is similar to what happens in an isolated inorganic molecule.

But are the clumpings of levels in the $Mn_2P_2^{2-}$ layer really behaving the way we expect? We can do some analytical detective work on the DOS. First we can decompose it into the part that is on Mn and the part that is on P. This is done in Figure 4, which in the solid-state trade is called a projection of the DOS on Mn or the local DOS on Mn. What is not on Mn is, of course, on P. Clearly the lower bands are mainly P, the higher ones are mainly Mn.

What about the bonding characteristics predicted in the qualitative bonding scheme of Figure 1? We have devised a bonding index called COOP, technically the overlap population weighted density of states,[27] which allows us to investigate this.

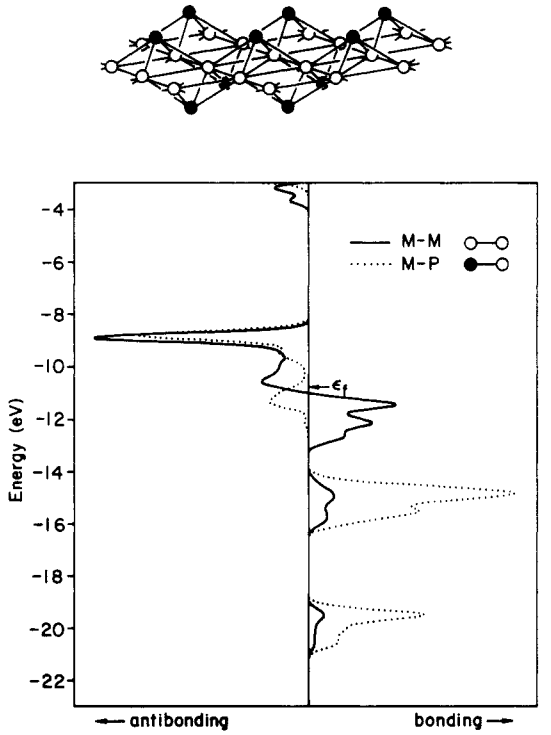

Figure 5. Crystal orbital overlap population curves for the Mn–Mn bonds (solid line) and Mn–P bonds (dotted line) in the $Mn_2P_2^{2-}$ single layer.

All the states in a given energy interval are interrogated as to their bonding character (as measured by an overlap population) and the resulting curve plotted as a function of energy. The integral of this COOP curve, which has positive (bonding) and negative (antibonding) regions, up to the Fermi level gives the total overlap population.

Figure 5 shows Mn–P and Mn–Mn COOP curves for the Mn_2P_2 layer. Note that the two lower bands (at −15 and −19 eV), which by the previous decomposition were seen to be mainly P,

(27) Some other applications of the COOP curves may be found in: (a) Wijeyesekera, S. D.; Hoffmann, R. *Organometallics* **1984**, *3*, 949. (b) Kertesz, M.; Hoffmann, R. *J. Am. Chem. Soc.* **1984**, *106*, 3453. (c) Saillard, J.-Y.; Hoffmann, R. *Ibid.* **1984**, *106*, 2006.

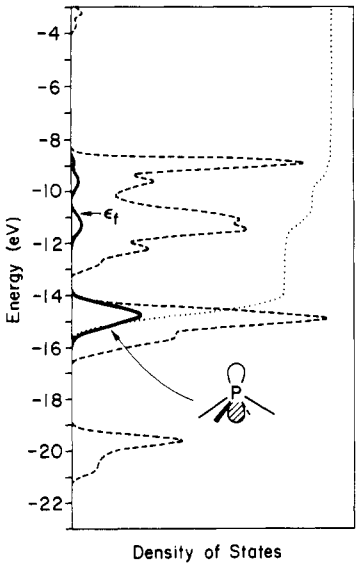

Figure 6. Phosphorus $3p_z$ orbital contribution (dark line) to the total DOS (dashed line) of the $Mn_2P_2^{2-}$ single layer. The dotted line is the integrated $3p_z$ DOS.

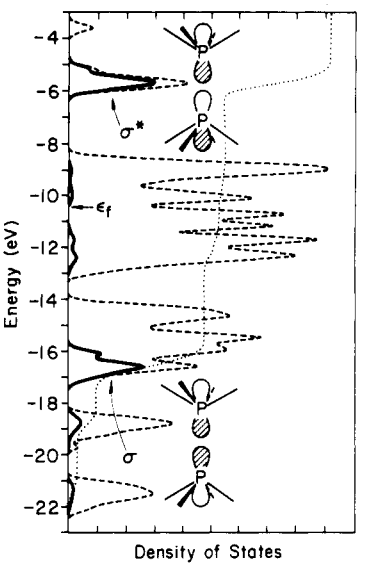

Figure 7. Phosphorus $3p_z$ orbital contribution (dark line) to the total DOS (dashed line) of the three-dimensional $Mn_2P_2^{2-}$ lattice, without the cation. The phosphorus–phosphorus bond length here is 2.4 Å. The dotted line is the integrated $3p_z$ DOS.

are Mn–P bonding, whereas the mainly metal bands around −12 eV are Mn–P nonbonding. The bunch of levels at ∼−9 eV is Mn–P antibonding—it corresponds to the crystal-field-destabilized t_2 level in Figure 1. The bottom of the mainly metal band is Mn–Mn bonding, the top Mn–Mn antibonding.

Everything is as expected. And it could not be otherwise, for there is no new physics in the bonding in the infinite solid that is not there in the discrete molecule.

Three-Dimensional $Mn_2P_2^{2-}$

In preparation for putting the $Mn_2P_2^{2-}$ layers together, let us look at the bonding situation around P. Each phosphorus in a two-dimensional slab is in an unusual coordination environment, **5** at the apex of a square pyramid of four Mn atoms. Such

5

four-coordinate pyramidal phosphido groups are as far as we know unknown,[28] though they have been suggested theoretically.[29] One would expect something like a localized lone pair at P pointing away from the Mn atoms. One can look for this by asking for the contribution of P $3p_z$ to the total DOS, Figure 6. The $3p_z$ orbital is indeed very well localized in a band at ∼−15 eV, >70% of the $3p_z$ being in that region.

On to the three-dimensional solid. When the two-dimensional $Mn_2P_2^{2-}$ layers are brought together to form the three-dimensional solid ($Mn_2P_2^{2-}$, still without the counterions), the P $3p_z$ orbitals or lone pairs in one layer form bonding and antibonding combinations with the corresponding orbitals in the layers above or below. Figure 7 shows the P $3p_z$ density of states at interlayer P–P = 2.4 Å. The wide band at −8 to −12 eV is Mn 3d. Below and above this metal band are P bands, and in these quite well localized, are P–P σ and σ^* combinations, **6**. The bands are

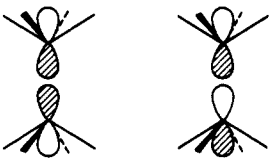

6

narrow because the lateral P–P distance is long, as **7**, a representation at the zone center of one of the two bands contributing to σ^*, shows.

If the three-dimensional calculation is repeated at different interslab or P···P distance all that happens is that the localized P–P σ and σ^* bands occur at different energies. Their splitting decreases with increasing P···P separation, as one would expect from their respective bonding and antibonding nature.

We are now in a position to explain simply the effect of the transition metal on the P–P separation. What happens when the transition metal moves to the right-hand side of the Periodic Table? The increased nuclear charge will be more incompletely screened and the d electrons more tightly bound. As a result, the d bands come down in energy and become narrower,[30] as shown

(28) A recent review on main-group heteroatoms in transition-metal clusters is: (a) Nicholls, J. N. *Polyhedron* **1984**, *3*, 1307. The closest analogue to the four-coordinate pyramidal group 15 atom is probably the M_4–N group in various M_4NL_{12} butterfly structures reported in: (b) Collins, M. A.; Johnson, B. F. G.; Lewis, J.; Mace, J. M.; Morris, J.; McPartlin, M.; Nelson, W. J. H.; Puga, J.; Raithby, P. R. *J. Chem. Soc., Chem. Commun.* **1983**, 689. (c) Braga, D.; Johnson, B. F. G.; Lewis, J.; Mace, J. M.; McPartlin, M.; Puga, J.; Nelson, W. J. H.; Raithby, P. R.; Whitmire, K. H. *Ibid.* **1982**, 1081. (d) Fjare, D. E.; Gladfelter, W. L. *Inorg. Chem.* **1981**, *20*, 3533. (e) Tachikawa, M.; Stein, J.; Muetterties, E. L.; Teller, R. G.; Beno, M. A.; Gebert, E.; Williams, J. M. *J. Am. Chem. Soc.* **1980**, *102*, 6648. Moreover, there are a few examples of four-coordinate pyramidal PR groups, P bonded to four metal atoms in a square-planar arrangement: (f) Ryan, R. C.; Dahl, L. F. *J. Am. Chem. Soc.* **1975**, *97*, 6904. (g) Lower, L. D.; Dahl, L. F. *Ibid.* **1976**, *98*, 5046. (h) Fernandez, J. M.; Johnson, B. F. G.; Lewis, J.; Raithby, P. R. *J. Chem. Soc., Chem. Commun.* **1978**, 1015. On the other hand, group 16 elements, mainly sulfur atoms, adopt this four-coordinate pyramidal geometry in many metal–sulfide clusters: (i) Pohl, S.; Saak, W. *Angew. Chem.* **1984**, *96*, 886. (j) Henkel, G.; Strasdeit, H.; Krebs, B. *Ibid.* **1982**, *94*, 204; *Angew. Chem., Int. Ed. Engl.* **1982**, *21*, 201. (k) Strasdeit, M.; Krebs, B.; Henkel, G. *Inorg. Chem.* **1984**, *23*, 1816. (l) Hagen, K. S.; Watson, A. D.; Holm, R. H. *J. Am. Chem. Soc.* **1983**, 105, 3905. (m) Christou, G.; Hagen, K. S.; Holm, R. H. *Ibid.* **1982**, *104*, 1744. Christou, G.; Hagen, K. S.; Bashkin, J. K.; Holm, R. H. *Inorg. Chem.* **1985**, *24*, 1010. (n) Vahrenkamp, H. *Angew. Chem.* **1975**, *87*, 363; *Angew. Chem., Int. Ed. Engl.* **1975**, *14*, 322. Similar coordinations for sulfur are also found in minerals such as pentlandite, bartonite, and djerfisherite: (o) Rajamani, V.; Prewitt, C. T. *Can. Miner.* **1973**, *12*, 198. (p) Hall, S. R.; Stewart, J. M. *Ibid.* **1973**, *12*, 169. (q) Evans, H. T., Jr.; Clark, J. R. *Am. Miner.* **1981**, *66*, 376. (r) Tani, B. S. *Ibid.* **1977**, *62*, 819. (s) Vaughan, D. J.; Craig, J. R. "Mineral Chemistry of Metal Sulfides"; Cambridge University Press: Cambridge, 1978.

(29) Minkin and Minyaev have shown that the pyramidal $C_4H_4P^+$ is at a local potential energy minimum. The isolobal analogue would be $[Co(CO)_3]_4P^+$ or its isoelectronic compounds. See: (a) Minkin, V. I.; Minyaev, R. M. *Usp. Khim.* **1982**, *51*, 586; *Russ. Chem. Rev.* **1982**, *51*, 332. (b) Minyaev, R. M.; Minkin, V. I. *Zh. Org. Khim.* **1982**, *18*, 2009.

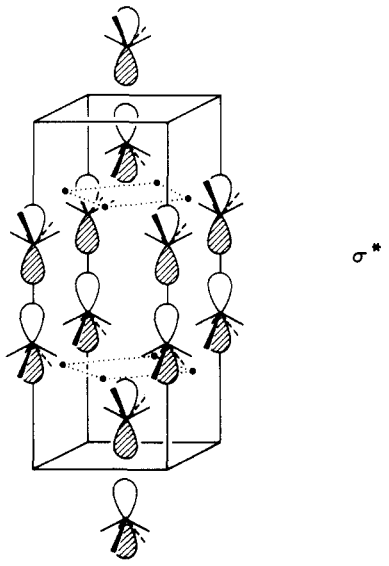

7

in **8**. At the same time the band filling increases. Two factors

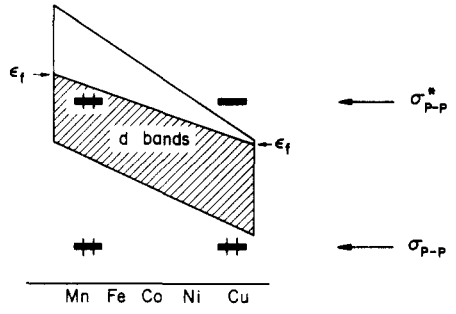

8

thus compete to determine the trend in the Fermi level, and it turns out that the first, the strength of the d-electron binding, wins out. The Fermi level sinks as one moves to the right, and the work function increases.

Now imagine superimposed on this variable energy sea of electrons the P–P σ and σ^* bands for some typical, moderately bonding P–P distance. On the left of the transition series the metal Fermi level is above the P–P σ^*. Both σ and σ^* are occupied, and there is no resultant P–P bond. As P–P stretches in response the σ^* only becomes more filled. On the right side of the transition series the P–P σ^* is above the Fermi level of the metal, and so is unfilled. The filled P–P σ makes a P–P bond. Making the P–P distance shorter only improves this situation.

Another way to put this is to think in terms of the Zintl concept[1b,31] of a full P–P bond and diatomic P_2^{4-}, **9**, in compounds

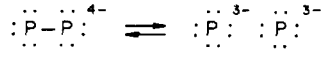

9 10

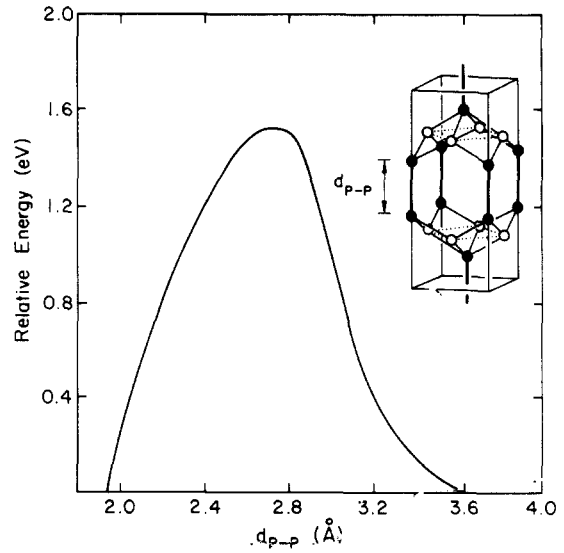

Figure 8. Relative energy per unit cell of the three-dimensional $Mn_2P_2^{2-}$ lattice as a function of phosphorus–phosphorus distance.

TABLE III: Extended Hückel Parameters

orbital	H_{ii}, eV	ζ_1[a]	ζ_2	c_1[a]	c_2
Mn 3d	−11.67	5.15	1.7	0.5140	0.6930
4s	−9.75	1.8			
4p	−5.89	1.8			
P 3s	−18.6	1.8			
3p	−14.0	1.8			

[a] Exponents and coefficients in a double ζ expansion of the 3d orbital.

of the late transition metals. As one moves to the left in the transition series one reduces the P_2^{4-} molecule to P_2^{6-}, breaking the σ bond. Alternatively, starting from two isolated phosphide ions (**10**) in compounds of the middle of the transition series, the metal oxidizes two such ions to form a diatomic P_2^{4-}. Either way, in any of a number of complementary pictures, *what we have before us is the remarkable phenomenon of the tunable breaking and making of a diatomic bond in the solid state.*

Let us examine the bond formation in a little more detail. Figure 8 shows the total energy per unit cell as a function of P–P separation. Note a maximum with two low energy regions on each side. The energy keeps dropping on the short P–P side, and there is a double minimum, whereas all the known compounds have a single one. These anomalies could be the result of deficiencies of the extended Hückel method, but actually they are not—they result from omitting the A^{2+} cations in these calculations. The counterions provide a Madelung energy to hold the slabs together on the long P···P side, and through their large size a countervailing force keeping the slabs apart on the short P···P side. Schematically these effects are shown in **11**.

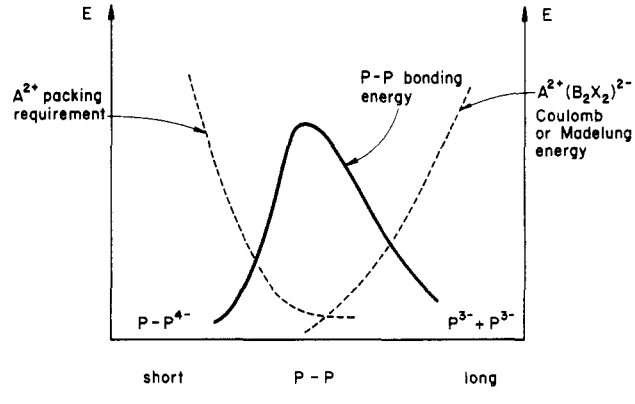

11

(30) For bulk metals theoretical calculations give ~1 eV difference in Fermi levels between Mn and Ni. See ref 27c and: (a) Shustorovich, E.; Baetzold, R. C.; Muetterties, E. L. *J. Phys. Chem.* **1983**, *87*, 1100. (b) Baetzold, R. C. *Solid State Commun.* **1982**, *44*, 781. Varma, C. M.; Wilson, A. J. *Phys. Rev. B* **1980**, *22*, 3795. Andreoni, W.; Varma, C. M. *Ibid.* **1981**, *23*, 437. The difference in work function between Mn and Cu is ~1 eV; see: (c) "Handbook of Thermionic Properties"; Samsanov, G. V., Ed.; Plenum Press Data Division: New York, 1966. Michaelson, H. B. *J. Appl. Phys.* **1977**, *48*, 4729.

The position of the P–P bonding curve is the main variable factor here. The maximum in the curve could be thought of as the point of maximum σ^* filling before the electrons flow from σ^* to the metal. And this point moves to the right (longer P–P distance) as the metal Fermi level falls. Anyway the "bonding", "Coulomb", and "packing" requirements combine in the known AB_2X_2 structures to give a single minimum, *either* a made *or* a broken P–P bond. We think that for some compounds in this series, for some choice of atoms, there will in fact exist two minima; i.e., a possible phase transition is predicted. We would recommend a study of these materials under pressure along the *c* axis.[35]

Acknowledgment. We are grateful to the National Science Foundation for its support of this work through Grant CHE 8406119 and Grant DMR 8217227 A02 to the Materials Science Center at Cornell University. Thanks are due to the members of our research group. C.Z. especially thanks Tim Hughbanks and Sunil Wijeyesekera for sharing their expertise with him. Appreciation is also due to Dr. Jerome Silvestre for providing us with some structural information. We thank Cora Eckenroth for the typing and Jane Jorgensen and Elisabeth Fields for the drawings.

Appendix

The extended Hückel method was used in all calculations.[32] Table III lists the parameters used for Mn and P. The geometry is chosen such that Mn is at the center of an ideal P_4 tetrahedron, Mn–Mn = 2.8284, Mn–P = 2.45Å. A 14K point set is used in the irreducible wedge in the Brillouin zone[33] to calculate average properties.

Registry No. $ThCr_2Si_2$, 12018-25-6; Si, 7440-21-3.

(31) See: Klemm, W. *Proc. Chem. Soc. London* **1958**, 329. Schäfer, H.; Eisenmann, B.; Müller, W. *Angew. Chem., Int. Ed. Engl.* **1973**, *12*, 694 and references therein.

(32) Hoffmann, R. *J. Chem. Phys.* **1963**, *39*, 1397. Hoffmann, R.; Lipscomb, W. N. *Ibid* **1962**, *36*, 2179, 3489; **1962**, *37*, 2872. Ammeter, J. H.; Bürgi, H.-B.; Thibeault, J. C.; Hoffmann, R. *J. Am. Chem. Soc.* **1978**, *100*, 3686.

(33) Pack, J. D.; Monkhorst, H. J. *Phys. Rev. B* **1977**, *16*, 1748.

(34) In this paper the periodic group notation is in accord with recent actions by IUPAC and ACS nomenclature committees. A and B notation is eliminated because of wide confusion. Groups IA and IIA become groups 1 and 2. The d-transition elements comprise groups 3 through 12, and the p-block elements comprise groups 13 through 18. (Note that the former Roman number designation is preserved in the last digit of the new numbering: e.g., III→3 and 13.)

(35) A number of high-pressure-induced physical property changes have been observed, many of them attributed to the valence change of A in AB_2X_2. (a) Eu valence change in $EuPd_2Si_2$: Röhler, J.; Krill, G.; Kappler, J. P.; Ravet, M. F.; Wohlleber, D. In ref 3a, p 215. Schmiester, G.; Perscheid, B.; Kaindl, G.; Zukrowsky, J. *Ibid.* p 219. (b) $\rho(p)$, linear compressibility and thermal expansion of $EuPd_2Si_2$: Batlogg, B.; Jayaraman, A.; Murgai, V.; Grupta, L. C.; Parks, R. D. *Ibid.* p 229. (c) $\rho(p)$, $T_c(p)$, $H_{c2}(p)$ of $CeCu_2Si_2$: Bellarbi, B.; Benoit, A.; Jaccard, D.; Mignot, J. M. *Phys. Rev. B* **1984**, *30*, 1182. Aliev, F. G.; Brandt, N. B.; Moshchalkov, V. V.; Chudinov, V. V.; *Solid. State Commun.* **1983**, *45*, 215. Aliev, F. G.; Brandt, N. B.; Lutsiv, R. V.; Moshchalkov, V. V.; Chudinov, S. M. *JETP Lett.* **1982**, *35*, 539. Aliev, F. G.; Brandt, N. B.; Levin, E. M.; Moshchalkov, V. V.; Chudinov, S. M.; Yasnitskii, R. I. *Sov. Phys.-Solid State* **1982**, *24*, 164. (d) Mössbauer studies on $NpCo_2Si_2$, hyperfine field $B_{eff}(p)$, isomer shift $S(p)$. Néel temperature $T_N(p)$: Potzel, W.; Moser, J.; Kalvius, G. M.; de Novion, C. H.; Spirlet, J. C.; Gal, J. *Phys. Rev. B* **1981**, *24*, 6762. Potzel, W. *Phys. Scr.* **1982**, *T1*, 100.

ARTICLES

Time-Dependent Fluorescence Solvent Shifts, Dielectric Friction, and Nonequilibrium Solvation in Polar Solvents

G. van der Zwan† and James T. Hynes*

Department of Chemistry, University of Colorado, Boulder, Colorado 80309 *(Received: July 25, 1984; In Final Form: June 13, 1985)*

The dynamics of time-dependent fluorescence (TDF) shifts subsequent to electronic absorption by a solute in polar solvents is discussed. It is shown that the TDF shift is directly proportional to the time-dependent dielectric friction $\zeta(t)$ on the absorbing molecule. This relationship points to the possibility of direct experimental determination of $\zeta(t)$. In addition, several approximate models which go beyond a simple Debye description are discussed. These models include solvent inertia and solvent polarization relaxation via translation and suggest that non-Debye behavior in TDF shifts might be observable. The connection of the TDF shift to related nonequilibrium solvation effects in chemical reactions in polar solvents is briefly described.

I. Introduction

The concept of dielectric friction—the measure of the dynamic interaction of a charge or dipole with the surrounding polar solvent—has played a central role over the years in discussions of ionic mobility and dipolar orientational relaxation. An admirable review of the concept and its applications is given by Wolynes.[1] Our own interest in dielectric friction is in a different and novel arena. In recent years, we have related this concept to dynamic polar solvent effects on charge transfer and dipole isomerizations in solution.[2-5]

Despite the intense interest in dielectric friction, its precise role and quantification have proved elusive[1]—a melancholy tribute to the difficulty of producing a tractable and accurate theoretical

† Present address: Department of Chemistry, University of Oregon, Eugene, OR 94703.

(1) P. G. Wolynes, *Ann. Rev. Phys. Chem.* **31**, 345 (1980).
(2) G. van der Zwan and J. T. Hynes, *J. Chem. Phys.*, **76**, 2993 (1982).
(3) G. van der Zwan and J. T. Hynes, *Chem. Phys. Lett.*, **101**, 367 (1983).
(4) G. van der Zwan and J. T. Hynes, *J. Chem. Phys.*, **78**, 4174 (1983); *Chem. Phys.*, **90**, 21 (1984).
(5) G. van der Zwan and J. T. Hynes, to be submitted.

0022-3654/85/2089-4181$01.50/0